SELF-ALIGNED 1.14-GHZ VIBRATING RADIAL-MODE DISK RESONATORS

Jing Wang, Zeying Ren, and Clark T.-C. Nguyen

Center for Integrated Wireless Microsystems (WIMS)
Dept. of Electrical Engineering and Computer Science, University of Michigan
Ann Arbor, Michigan 48109-2122 USA
Tel: (734)764-3352, Fax: (734)763-9324, e-mail: jingw@engin.umich.edu

ABSTRACT

A new fabrication methodology that allows self-alignment of a micromechanical structure to its anchor(s) has been utilized to achieve vibrating radial-contour mode micromechanical disk resonators with record resonance frequencies up to 1.14 GHz and measured Q's at this frequency >1,500 in *both vacuum and air*. In addition, 733-MHz versions have been demonstrated with Q's of 7,330 and 6,100 in vacuum and air, respectively. For these resonators, self-alignment of the stem to exactly the center of the disk it supports allows balancing of the resonator far superior to that achieved by previous versions (where separate masks were used to define the disk and stem), allowing the present devices to retain high Q while achieving frequencies in the GHz range for the first time.

I. INTRODUCTION

With Q's often exceeding 10,000, vibrating micromechanical ("μmechanical") resonators are emerging as viable candidates for on-chip versions of the high-Q resonators used in wireless communication systems for frequency generation and filtering [2]. However, the acceptance of such devices in present-day communication transceivers is so far still hindered by several remaining issues, including: (1) a frequency range that so far has not reached 1 GHz; (2) the need for vacuum to attain high Q; and (3) impedance values higher than normally exhibited by macroscopic high-Q resonators.

This work now alleviates the first two of the above issues. In particular, micromechanical radial contour-mode vibrating disk resonators featuring new self-aligned stems have been demonstrated with record resonance frequencies up to 1.14 GHz and measured Q's at this frequency >1,500 in *both vacuum and air*. In addition, 733-MHz versions have been demonstrated with Q's of 7,330 and 6,100 in vacuum and air, respectively. For these resonators, self-alignment of the stem to exactly the center of the disk it supports allows balancing of the resonator far superior to that achieved by previous versions (where separate masks were used to define the disk and stem [1]), allowing the present devices to retain high Q while achieving frequencies in the GHz range for the first time. In addition, the use of more rugged polysilicon electrodes (as opposed to the malleable metal used in previous disks [1]) greatly improves the yield of these devices, and the introduction of a substrate ground plane greatly facilitates the measurement of their UHF frequency characteristics.

II. DEVICE STRUCTURE, OPERATION & MODELING

Figure 1 presents the perspective-view schematic of a self-aligned disk resonator in a typical two-port bias, excitation, and measurement scheme, with the tops of its electrodes rendered transparent to enable viewing of underlying structure. As illustrated, this device consists of a 2μm-thick polysilicon disk suspended by a 2μm-diameter stem self-aligned to its center and enclosed by two polysilicon electrodes spaced less
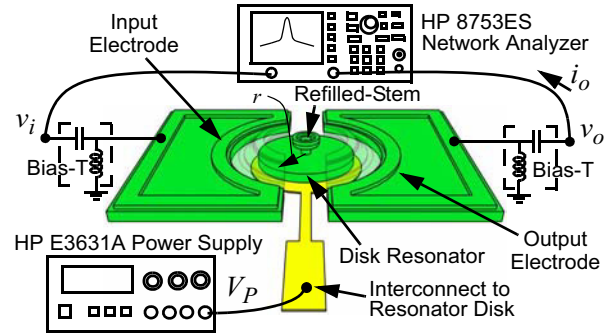

Fig. 1: Perspective-view schematic of a self-aligned disk resonator identifying key features and a two port measurement scheme.

than 1000Å from the disk perimeter. To excite this device in its two-port configuration, a dc-bias voltage V_P is applied to the disk, and an ac signal v_i to its input electrode, generating an electrostatic force acting radially on the disk at the frequency of the ac input. When the frequency of v_i matches the radial contour-mode resonance frequency of the disk, the resulting force drives the disk into a vibration mode shape where it expands and contracts radially around its perimeter, in a fashion reminiscent of "breathing". This motion creates a dc-biased (by V_P) time-varying capacitance between the disk and output electrode that then sources an output current i_o proportional to the amplitude of vibration.

The dimensions needed to attain a specified resonance frequency f_o for a radial contour-mode disk resonator can be obtained by solving the mode frequency equation [3]:

$$\delta \times \frac{J_0(\delta)}{J_1(\delta)} = 1 - \sigma \tag{1}$$

where

$$\delta = \omega_o R \sqrt{\frac{\rho(1-\sigma^2)}{E}}, \tag{2}$$

and where R is the disk radius; $\omega_o = 2\pi f_o$ is its angular resonance frequency; $J_n(y)$ is the Bessel function of the first kind of order n; and ρ, σ, and E are the density, Poisson ratio, and Young's modulus, respectively, of the disk structural material. Note that the above formulas serve as a correction to the frequency equations presented by [1], which were in error.

Despite its mechanical nature, the disk resonator of Fig. 1 still behaves like an electrical device when looking into its ports, and so can be modeled by any one of the electrical *LCR* equivalent circuits shown in Fig. 2. The element values in these circuits are governed by the total integrated kinetic energy in the resonator, its mode shape, and parameters associated with its transducer ports [4]. Using the procedure of [5], the expressions for equivalent inductance L_x, capacitance C_x, and resistance R_x, for the purely electrical version of the equivalent circuit (i..e, Fig. 2(b)) can be written as
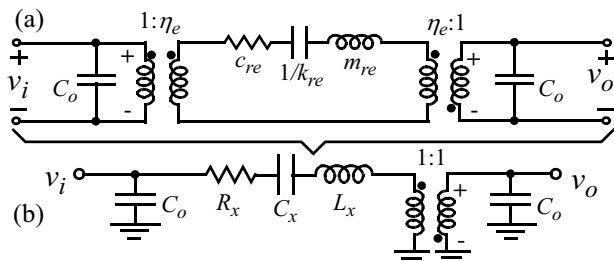
947

Fig. 2: Equivalent circuit models for a two-port disk resonator. (a) Physically consistent model using actual values of mass and stiffness for elements. (b) Purely electrical model.

$$L_x = \frac{m_{re}}{\eta_e^2} \qquad C_x = \frac{\eta_e^2}{k_{re}} \qquad R_x = \frac{\omega_o m_{re}}{Q \, \eta_e^2} \qquad (3)$$

where

$$m_{re} = \frac{2\pi\rho t \int_0^R r J_1^2(hr)dr}{J_1^2(hR)} \;, \; h = \sqrt{\frac{\omega_o^2 \rho}{\left(\frac{2E}{2+2\sigma} + \frac{E\sigma}{1-\sigma^2}\right)}} \quad (4)$$

$$\eta_e = V_P\left(\frac{\partial C}{\partial r}\right) \;, \; k_{re} = \omega_o^2 m_{re} \qquad (5)$$

and where m_{re} and k_{re} are the effective equivalent mass and stiffness, respectively, of the disk in its radial-contour mode, and t is thickness. These expressions also correct errors in [1].

One important difference between the stiff, high frequency resonators of this work and previous lower frequency ones is the difference in total energy per cycle. In particular, the peak kinetic energy per cycle can be computed via the expression

$$KE_{peak} = \frac{1}{2}m_{re}(\omega_o X)^2 = \frac{1}{2}k_{re}X^2 , \qquad (6)$$

where X and k_{re} are the peak displacement and effective stiffness, respectively, at the disk location across from the center of an electrode. Given that the $k_{re} \sim 73.5$ MN/m for a 1.14-GHz disk resonator is more than 49,000X the 1,500 N/m of a 10-MHz clamped-clamped beam, the former is expected to store 49,000X more energy per cycle for the same displacement amplitude. With energies per cycle many times larger than those lost to viscous gas damping, the resonators of this work, and virtually any high stiffness, high frequency μmechanical resonator device, are expected to exhibit high Q even under air damped conditions.

III. STEM SIZE AND PLACEMENT

As mentioned, the key feature of this work that allows radial contour-mode disk resonators to achieve frequencies >1 GHz with exceptional Q is self-alignment (i.e., exact placement) of the stem at the very center of the disk. To illustrate the importance of perfect alignment, Fig. 3 presents ANSYS modal analyses on a 20μm-diameter radial-contour mode disk with a 2μm-diameter stem for the cases of (a) a perfectly centered stem; and (b) a stem offset from the center by only 1 μm. Here, a perfectly centered stem leads to a symmetric and purely radial 2nd contour mode shape. Conversely, even just 1 μm of misalignment leads to dramatic mode shape distortions and consequent acoustic energy losses to the substrate that lower the Q, making resonance detection difficult.

In addition to misalignment, the finite diameter of the stem also significantly impacts the achievable Q. In particular, since the node at the disk center exists only at a single infinitesi-
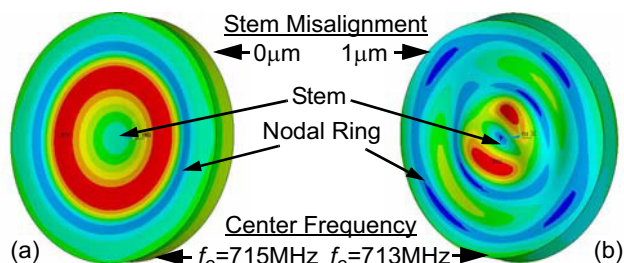

Fig. 3: ANSYS modal displacement simulation for a 20μm-diameter, 2μm-stem, radial-contour mode disk for the cases of (a) perfectly centered stem; and (b) a stem offset from the center by only 1μm.
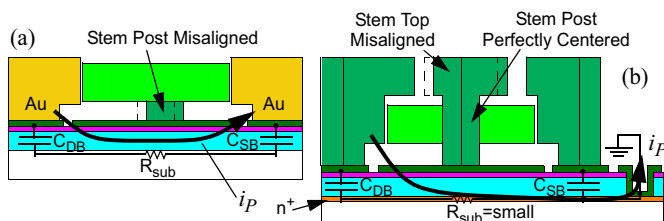

Fig. 4: Comparison between (a) a previous disk process; and (b) the new self-aligned disk process, each with the same amount of misalignment. Here, misalignment in (a) leads to stem misalignment, but only stem top misalignment in (b), which does not lower Q. In addition, use of a contacted substrate ground plane in (b) prevents feedthrough current i_P from reaching the output electrode, making resonance detection easier.

mally small point, and motion still occurs at locations immediately outside that point, the presence of a finite-width stem attempting to restrict that motion results in further energy dissipation. The higher the mode, the closer the high velocity points to the stem edges, and the greater the likelihood that even disks with perfectly centered stems still suffer Q degradation. As a result, high Q at high frequency is best achieved with thinner stems.

IV. SELF-ALIGNED STEM FABRICATION PROCESS

Given the importance of stem alignment described above, the fabrication process of this work is designed to eliminate the possibility of disk-to-stem misalignment, by removing the need for alignment. In particular, instead of using an anchor mask to first define the stem, then another mask aligned to the first to define the disk around the stem, as was done in a previous metal-electrode disk resonator process [6], the present process defines both the stem position and disk edges all in one mask, effectively eliminating the possibility of misalignment. An additional difference between this process and the previous is the inclusion of a contactable substrate ground plane, which proves instrumental in suppressing feedthrough currents to allow clean measurement of GHz vibrating disk frequency characteristics. Figure 4 summarizes the differences between the present self-aligned process and its predecessor.

Figure 5 presents cross-sections and associated scanning electron micrographs (SEM's) summarizing the process flow that achieves self-aligned-stem disk resonators. Right at the outset, the process differs from [6], in that it starts with a heavy phosphorous diffusion to serve as the substrate ground plane mentioned above. This is followed by polysilicon surface micromachining steps similar to those used in the process of [6] up to the point of defining the disk structure. Specifically, a 2μm-thick LPCVD high-temperature oxide (HTO) film is first deposited at 920°C using a $SiCl_2H_4/N_2O$-based recipe over the n^+-doped substrate, followed by a 3500Å-thick

TRANSDUCERS '03
The 12th International Conference on Solid State Sensors, Actuators and Microsystems, Boston, June 8-12, 2003
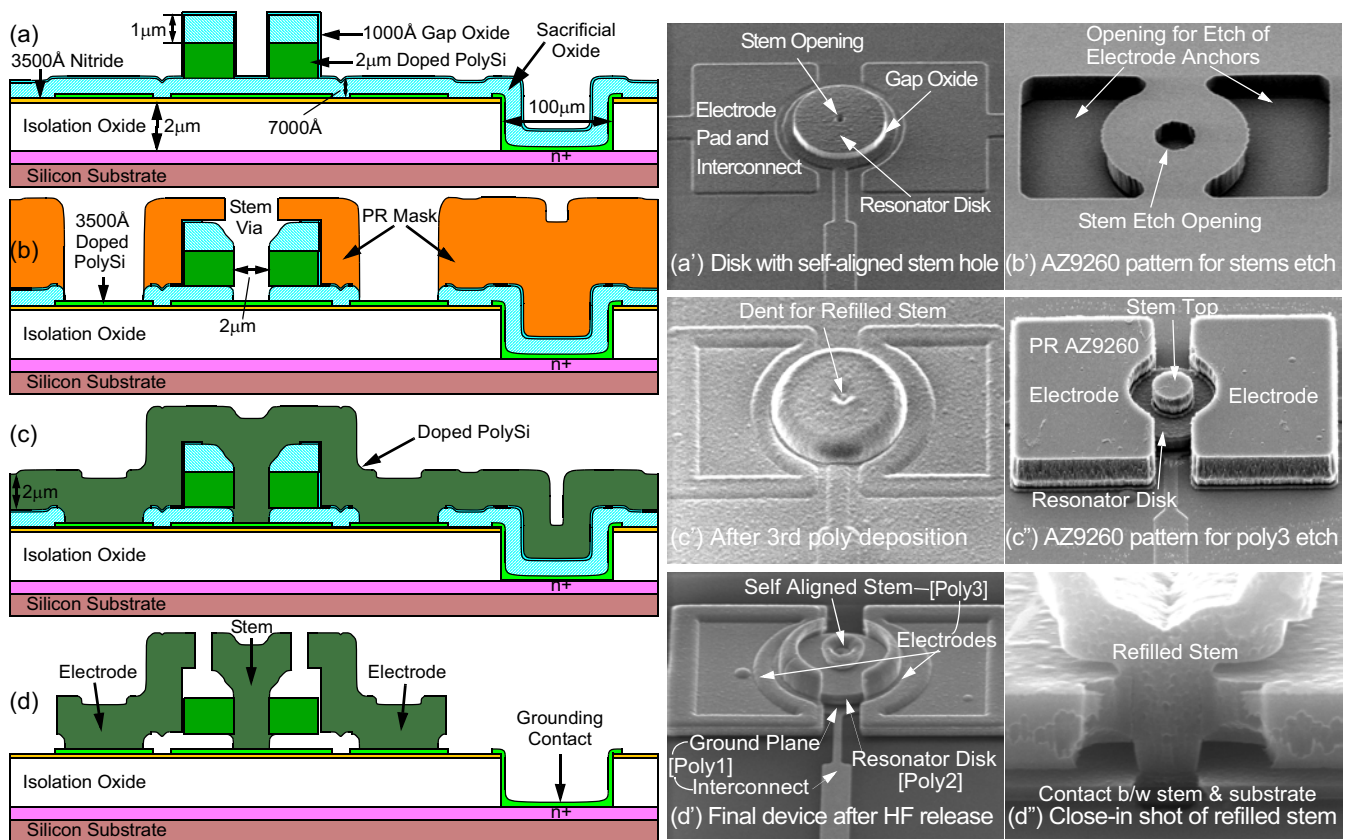
948

Fig. 5: Fabrication process flow for stem self-aligned radial-contour-mode disk resonators, featuring a substrate ground plane to suppress parasitic feedthrough. (a)-(d) Cross-sectional diagrams for this process. (a')-(d") SEM's at different stages of the process.

film of LPCVD Si_3N_4, and these two layers together serve to isolate devices and interconnects from the conductive silicon substrate. Next, 100μm×100μm substrate contact trenches are dug by a combination of dry and wet etches through the oxide/nitride isolation layers. Interconnect polysilicon is then deposited via LPCVD to a thickness of 3500Å and $POCl_3$-doped. After patterning this polysilicon layer to form ground planes, interconnects, and substrate contact pads, 8000Å of LPCVD HTO is deposited to act as a sacrificial layer to temporarily support a subsequent structural polysilicon layer during its own deposition and patterning. The structural polysilicon film is deposited 2μm-thick via LPCVD at 588°C, at which temperature a low-stress, fine-grained material is achieved. This film is $POCl_3$-doped, then capped with a 1μm-thick film of HTO that serves as both a hard mask during etching of the structural polysilicon film, and later as a spacer layer to separate the disk from overhanging electrode portions.

Before etching, the structural polysilicon is annealed in N_2 at 1050°C for 1 hour to activate dopants and relieve residual stress—an important step that insures a high Q structural material. Then, in another substantial deviation from [6], the composite oxide mask/polysilicon layer is patterned *in a single mask* to define not only the disk structure, but also a 2μm-diameter opening at its center that defines the eventual location of the stem. Here, the oxide hard mask is patterned and plasma etched to the desired device geometries, and these patterns are then transferred to the underlying structural polysilicon layer via a high density plasma ICP process, using a SF_6/C_4F_8 chemistry to insure vertical sidewalls. A 1000Å-thick LPCVD sidewall sacrificial HTO film is then conformally deposited to define the eventual electrode-to-resonator capaci-

tive gap spacing, yielding the cross-section of Fig. 5(a)(a'). Pursuant to eventual refilling of the stem opening, a 6.6μm-thick AZ9260 photoresist (PR) is spun and patterned to expose the stem and the electrode vias, after which the sidewall sacrificial spacer oxide is removed in the stem opening and the underlying bottom sacrificial oxide etched down to the substrate via a combination of wet and dry etches (c.f., Fig. 5(b)(b')). With exposed stem holes and electrode anchor vias, a subsequent (third) 2μm LPCVD low-stress polysilicon deposition then not only provides the material for electrodes, but also refills the anchor vias to create very rigid, self-aligned stems (c.f., Fig. 5(c)(c')). This third polysilicon layer is then $POCl_3$-doped and annealed in N_2 at 1050°C for 1 hour.

To define electrodes, a layer of AZ9260 photoresist is next spun 6.6μm-thick to completely submerge the structural polysilicon topography deep under the quasi-planarized photoresist film. After exposing and developing the photoresist (c.f., Fig. 5(c")), then patterning the top polysilicon to define stem tops and electrodes, structures are released in 49% concentrated HF to yield the final cross-section of Fig. 5(d)(d'). Figure 5(d") shows a close-up cross-sectional SEM visually verifying that the refilled stem is solidly attached to both the underlying substrate and the inner disk sidewalls.

V. EXPERIMENTAL RESULTS

As mentioned in the introduction, μmechanical resonators often exhibit port-to-port impedances much larger than conventional macroscopic devices. Nevertheless, despite large impedance mismatching, a direct two-port measurement set-up, such as shown in Fig. 1, was sufficient to obtain frequency and Q data in most cases. For cases where impedance-mis-

TRANSDUCERS '03
The 12th International Conference on Solid State Sensors, Actuators and Microsystems, Boston, June 8-12, 2003

949

732.9MHz (In Vacuum), Q=7330

V_P=6.17V
v_{IF}=7V
v_{RF}=2.24V

(a) Frequency [MHz]

732.9MHz (In Air), Q=6100

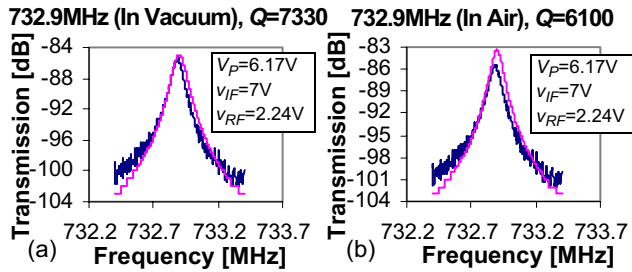V_P=6.17V
v_{IF}=7V
v_{RF}=2.24V

(b) Frequency [MHz]

Fig. 6: Measured (dark) and predicted (light) frequency characteristics for a 733-MHz, 2nd mode, 20μm-diameter disk resonator measured in (a) vacuum and (b) in air, using a mixing measurement setup.

1139.9MHz (In Vacuum), Q=1595

V_P=12.9V
v_{IF}=8.91V
v_{RF}7.94V

(a) Frequency [MHz]

1139.9MHz (In Air), Q=1583

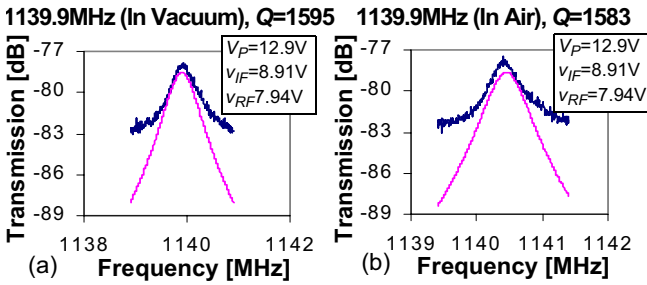V_P=12.9V
v_{IF}=8.91V
v_{RF}=7.94V

(b) Frequency [MHz]

Fig. 7: Measured (dark) and predicted (light) frequency characteristics for a 1.14-GHz, 3rd mode, 20μm-diameter disk resonator measured in (a) vacuum and (b) in air, using a mixing measurement setup.

Table I: Measured vs. Predicted Disk Modal Frequencies

Disk Diameter (μm)	1st mode (MHz)	2nd mode (MHz)	3rd mode (MHz)	4th mode (MHz)	5th mode (MHz)
36	152|152	402|406	639|645	875|872	1110|
21	261|260	689|683	1096|1095	1500|	1904|
20	274|273	725|733	1151|1140	1575|	1999|
16	343|342	904|	1439|	1969|	2499|
12	457|454	1206|	1918|	2626|	3331|

Legend:
Predicted Frequency(E=150GPa,σ=0.29,ρ=2.3kg/m^3) | Measured Frequency

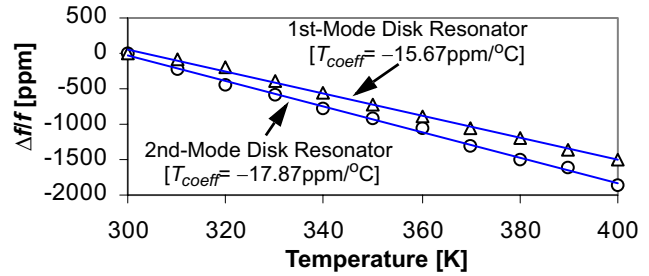1st-Mode Disk Resonator [T_{coeff}= −15.67ppm/°C]

2nd-Mode Disk Resonator [T_{coeff}= −17.87ppm/°C]

Fig. 8: Measured fractional frequency change versus temperature for 1st mode and 2nd mode 22μm-diameter disk resonators.

matches made direct two-port measurement impossible, a mixing-based measurement set-up was used that suppressed parasitic feedthrough by moving motional currents away from them in the frequency domain [7][8], allowing unimpeded measurement of devices. In either case, it should be noted that losses seen in the measured spectra to follow arise from impedance mismatching, and are not indicative of device loss. By their sheer high Q, it should be obvious that the devices should exhibit very little loss when used in properly matched filters [4][5].

Figures 6 and 7 present frequency spectra measured via a mixing set-up for the device of Fig. 5(d') operating in its second radial-contour mode at 733 MHz, with a Q of 7,330 in vacuum and 6,100 in air; and in its third radial contour mode at 1.14 GHz with Q's of 1,595 and 1,583, in vacuum and air, respectively. (It should be noted that due to impedance mismatching, the peak height in the latter measurement is quite small, so the extracted Q probably undershoots the actual value by a good amount.) Both measurements verify the prediction that the Q's of high stiffness, high frequency devices should remain high whether operated in vacuum or at atmospheric pressure. In addition to measured spectra (dark), theoretical curves (light) predicted using the device models are included in the plots, verifying the accuracy of the models. Table I presents a comparison of predicted and measured frequencies for different device sizes and modes, showing good agreement to within 1%.

Finally, Fig. 8 presents measured plots of fractional frequency change versus temperature for a 22μm-diameter disk resonator fabricated using the self-aligned process of Fig. 5 and operated in its fundamental and second modes. The uncompensated temperature coefficients of −15.67 ppm/°C and −17.87 ppm/°C for the fundamental and second modes, respectively, are fairly good relative to macroscopic counterparts at this frequency.

I. CONCLUSIONS

By eliminating anchor-to-disk misalignment error through self-alignment, the radial-contour mode polysilicon micromechanical disk resonators of this work have now achieved frequencies in excess of 1 GHz with Q's still >1,500. In addition, given that the 733-MHz disk achieved a frequency-Q product of 5.37×10^{12}, Q's of ~5,400 at 1 GHz should also be feasible, assuming a constant f_o-Q product. Furthermore, these high stiffness, high frequency devices attain almost the same high Q values whether operated in vacuum or air. The implications here are enormous, as this result effectively states that vacuum is no longer needed to attain exceptional Q in high frequency vibrating micromechanical resonators—a fact that should substantially lower the cost of devices based on vibrating RF MEMS technology, making them strong contenders in numerous wireless communication applications, provided impedance matching issues can be sufficiently alleviated.

References

[1] J. R. Clark, *et al.*, *Tech. Digest*, IEEE Int. Electron Devices Meeting, Dec. 11-13, 2000, pp. 399-402.

[2] C. T.-C. Nguyen, *Dig. of Papers*, Topical Mtg on Silicon Monolithic IC's in RF Systems, Sept. 12-14, 2001, pp. 23-32.

[3] M. Onoe, "Contour vibrations of isotropic circular plates," *J. Acoustic. Soc. Amer.*, vol. 28, pp1158-1162, Nov. 1956.

[4] R. A. Johnson, *Mechanical Filters in Electronics*. New York, NY: Wiley, 1983.

[5] F. D. Bannon III, *et al.*, *IEEE J. Solid-State Circuits*, vol. 35, no. 4, pp. 512-526, April 2000.

[6] W.-T. Hsu, *et al.*, *Tech. Digest*, IEEE Int. Micro Electro Mechanical Systems Conf., Jan. 21-25, 2001, pp.349-352.

[7] Ark-chew Wong, *et al.*, *Tech. Digest*, IEEE Int. Electron Devices Meeting, Dec. 6-9, 1998, pp. 471-474.

[8] J. Wang, *et al.*, to be published in the *Proceedings* of the 2003 MTT-RFIC Symposium, June 8-10, 2003.

TRANSDUCERS '03
The 12th International Conference on Solid State Sensors, Actuators and Microsystems, Boston, June 8-12, 2003

950